Combining Volt-VAr and Watt-VAr Control in Smart Inverters to Mitigate Voltage Rise on Distribution Network

Muammar Zainuddin*‡, Muhammad Asri*, Frengki Eka Putra Surusa*, Andi Takdir*

* Department of Electrical Engineering, Faculty of Engineering, Universitas Ichsan Gorontalo, 96138 Gorontalo City-Indonesia

(muammarz@unisan.ac.id, muhammadasri@unisan.ac.id, frengki@unisan.ac.id, andiunisan@gmail.com)

‡ Corresponding Author; Muammar Zainuddin, 96138, Tel: +62 852 5866 7668, muammarz@unisan.ac.id

Received: 09.11.2023 *Accepted*:19.12.2023

Abstract- The high penetration of photovoltaic (PV) generators into the distribution network has an impact on voltage violations. Smart inverter (SI) functionality with reactive power capabilities has been introduced by providers to support grid voltage. Meanwhile, the inverter with reactive power controls requires a large power capacity and need to be effective under fluctuating power loads and intermittencies in solar PV. Therefore, this study aimed to investigate the performance of Volt-VAr and Watt-VAr control modes implemented on SI as well as to propose the combination to mitigate voltage rise. A comprehensive assessment was conducted on active and reactive power performance, as well as daily voltage profiles in PV system with due consideration for the solar irradiance and ambient temperature. Moreover, the case study was the multi-smart inverter PV system with a total power of 2,000 kW connected to the real distribution network in Gorontalo, Indonesia. A Quasi-dynamic simulation was applied based on power flow analysis to evaluate profiles for inverter loading, transformer loading index (TLI), and voltage deviation index (VDI) as well as the power losses. The proposed control combination was based on droop settings and focused on three different cases considered easy to implement. The results showed that PV system effectively generated active power daily and compensated for reactive power without overloading the inverter and transformer. Furthermore, the voltage network deviation index was significantly reduced from the initial value. The proposed control strategy effectively mitigates voltage rise during peak power.

Keywords : Inverter loading index, PV power losses, smart inverter, transformer loading index, voltage deviation index.

1. Introduction

Renewable energy sources are observed to have been developed significantly over the last decade globally. Specifically in Indonesia, the total capacity of renewable energy generator in the country was recorded to be 12,603 MW in 2022 [1]. Solar Photovoltaic (PV) resources also increased significantly even though the total installed power was very small compared to the potential of 200.1 GW. The Indonesian government was reported to be targeting a 55% capacity of PV and wind generator by 2040 [2] as shown through the massive promotion of energy conservation policies, PV electricity prices, business models, and network infrastructure development. However, several technical challenges need to be addressed by Distribution Network Operators (DNOs) and PV owners (PVOs) such as the identification of the microgrid flexibility solutions in grid development.

Future power systems are required to be flexible to accommodate different distributed energy resources (DERs). These DERs are popular for their ability to reduce voltage drops and power losses, improve power quality and network reliability, and maximize the energy potential of a region. However, one negative issue identified with this concept in recent years is the voltage rise in distribution network [3]–[5] which is causing non-compliance with grid codes [6]. One of the causative factors is the reverse power flow [7], [8] and this means there is a need to control PV generator in order to avoid voltage violations.

The conventional methods to maintain grid voltage with using transformer tap changer control or a voltage regulator in the line but both are not effective for active distribution network. The active power flow from PV system usually increases during peak solar radiation while the power demand during is relatively low, leading to overvoltage at the point of common coupling (PCC). The solution currently being

developed for microgrid flexibility is smart inverter (SI) technology. SI functionality offers local control's to support frequency and voltage regulation. Smart inverter's is normally rated in kilovolt-amperes instead of ordinary kilowatts in conventional inverters because it is designed to operate at unity power factor (PF 1). Furthermore, IEEE 1547-2018 standards recommend that DERs associations support grid voltage through reactive power capability [9]. This has made the Indonesian government establish standards in the form of an Indonesian grid code to integrate renewable energy into the power system [10].

SI provides active power control (APC) and reactive power control (RPC) functions with the main goal of mitigating over/undervoltage and frequency fluctuations in the electrical grid. Several studies evaluated these functions with some observed to focus on the Constant Power Factor (CPF) [11], [12] and Constant Reactive Power (CRP) control modes [13] as well as the PF(P) designed for RPC [14]. Moreover, inverters with P(V) operating on APC based on power curtailment as a function of grid voltage control were also investigated [15]–[17]. Some analyses also focused on Q(P) which was RPC operating as a function of active power [18]–[20] and Q(V) for RPC in grid voltage control [21]–[26]. All control modes PF(P), P(V), Q(P), and Q(V) are droop-control based but Q(V) or Volt-VAr was observed to be more acceptable to support grid voltage. Furthermore, voltage rise mitigation was proposed to use coordinated control schemes with a battery energy storage system and energy management (SI-BESS) [27]–[30], demand side management [31]–[33], grid reinforcement [34], and on-load tap changer transformers [35]–[37].

A coordinated control was also proposed for SI through the combination of Volt-VAr and Volt-Watt [38]–[40]. However, the control tended to create conflicts between active and reactive power priorities in maintaining voltage and required a fast execution response because the grid voltage was affected by two variables including the active or reactive power. The quantity of reactive power was observed to be limited depending on the inverter size. Karbouj et al. [41] reported that its reactive power capability was affected by solar irradiance and ambient temperature. Therefore, the reactive power of inverter was required to be limited because of inverter size and meteorological factors.

This study was conducted to investigate the performance of droop setting-based Volt-VAr and Watt-VAr controls as well as to propose a combination of these controls to mitigate overvoltage in distribution network. The process focused on varying the setting points for each control strategy. Moreover, quasi-dynamic simulations based on power flow analysis were used to measure the daily performance of active power, reactive power, and voltage in PV system. A comprehensive analysis was also conducted to assess the impact of RPC on maximum loading and voltage deviation index (VDI) as well as power system losses. Furthermore, the control strategies were simulated on multi-inverter PV generator with a total power of 2,000 kW connected to a medium voltage distribution network (MVDN) 43-bus system in Gorontalo, Indonesia. Quasy-dynamic simulation considers the daily profile of power loads.

2. Distribution Network with PV Power Plant

2.1. Active and Reactive Power of PV Power Plant

PV system are typically designed using single or multiple inverters while the panel array typically consists of series and parallel DC circuits. It is also important to state that the inverters is parallel to each other through a combiner panel connected to the transformer using low voltage (LV) cables. Medium and large-scale PV systems are also commonly connected to the grid using transformer. The output transformer is normally connected to the grid using medium voltage (MV) cable as shown in the simplified structure of grid-connected PV system in Figure 1. Meanwhile, all AC components are believed to be contributing to power losses which are required to be considered by the total active power (P_{PV}) and reactive power (Q_{PV}) values sent to the grid [42].

The active power of each inverter unit (P_{inv-i}) depends on the level of solar irradiance and ambient temperature, while the output reactive power of each inverter (Q_{inv-i}) relies on the local control of inverter but the amount is limited according to inverter power rating (S_{inv-i}). The maximum ability of the inverter to supply or absorb reactive power is expressed in mathematical Equation (1). Therefore, the total active power ($P_{tot.inv}$) and total reactive power ($Q_{tot.inv}$) of the multiple inverter is expressed using the following Equations (2) and (3):

$$Q_{inv-i}^{max} = |Q| \leq \sqrt{S_{inv-i}^2 - P_{inv-i}^2} \quad (1)$$

$$P_{tot.inv} = \sum_{i=1}^{n} P_{inv-i} \quad (2)$$

$$Q_{tot.inv} = \sum_{i=1}^{n} Q_{inv-i} \quad (3)$$

The power losses in each component of PV system can lead to the reduction of the total active and reactive power to be exported. Therefore, the total active and reactive power are formulated in Equations (4) and (5) respectively which are adopted from reference [42].

$$P_{PV} = P_{tot.inv} - P_{LV-cable} - P_{trx} - P_{MV-cable} \quad (4)$$

$$Q_{PV} = \pm Q_{tot.inv} \pm Q_{LV-cable} - Q_{trx} \pm Q_{MV-cable} \quad (5)$$

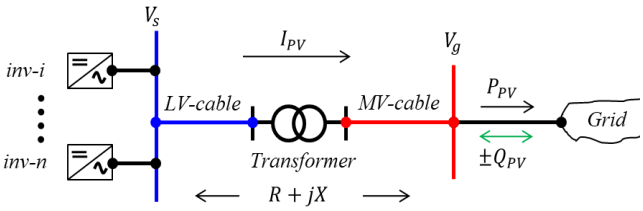

Fig. 1. Simplified structure of PV system connected to the grid.

Where, $P_{LV-cable}$ is the active power losses on the LV side, P_{trx} is the active power losses on transformer, and $P_{MV-cable}$ is the active power losses on the MV side. Moreover, the $Q_{LV-cable}$ is the reactive power losses on the LV side, Q_{trx} is the reactive power losses on transformer, and $P_{MV-cable}$ is the reactive power losses on the MV side. The ±

sign Is used to determine the inductive or capacitive status of the reactive power.

2.2. Voltage Rise Due to High Power PV Penetration

The basic principle associated with the power flow for grid-connected PV generator is its operation in parallel to other power sources in a single network. The power flow from the PV system into distribution network can cause a change in the amplitude and phase of the current, leading to voltage variations. Figure 1 shows that the total inverter power is delivered through the series impedance to the grid where V_s is the voltage at the sending bus with the same amplitude and phase, V_g is the supply voltage of PV system at PCC, R and X are the resistance and reactance values of the conductor components, respectively, and I_{PV} is the current flow from PV system to the grid. Moreover, the changes in the grid voltage are expressed using the following equation (6).

$$\Delta V = \frac{(P_{pv}+Q_{pv})^*}{V_g}(R + jX) \quad (6)$$

The effect of resistance can be neglected for systems with a low R/X ratios, leading to the expression of the change in voltage magnitude using the following equation (7).

$$\Delta V = \frac{Q_{pv}X}{V_g} + j\frac{P_{pv}X}{V_g} \quad (7)$$

The effect of resistance is significant in systems with a high R/X ratios, leading to the formulation of the change in voltage magnitude |ΔV| using equation (8).

$$|\Delta V| = \frac{P_{pv}R+Q_{pv}X}{V_g} \quad (8)$$

The voltage in distribution network can drop when the feeder load exceeds the power supply from the generator. It can also rise when power from PV system is more than the grid load. An increase in the voltage increases is considered abnormal when the allowable standards are exceeded and this is the reason SI is normally used to ensure compliance with the grid code.

2.3. Smart Inverters with Reactive Power Control

The ability of SI to regulate reactive power output based on droop control is one of the evolving functions. This is shown in the active and reactive power capability curve presented using the PQ quadrant in Figure 2. The red line shows the minimum limit of reactive power on DERs for category A, and the black line for category B according to the IEEE 1547-2018. It is also important to state that the control modes on SI have characteristic curves to be set according to applicable limits in IEEE 1547 standards for reactive power injection or absorption. Therefore, the characteristic curve and setting points used in this study are discussed in the following sections.

2.4. Impact Metrics

Smart inverters with reactive power control has technical and economic impacts on distribution system operations [43]. Therefore, each aspect was comprehensively assessed

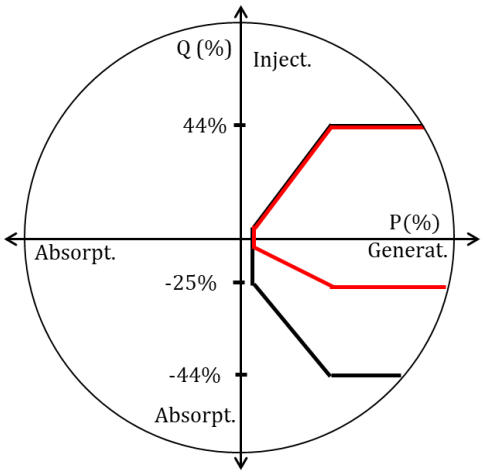

Fig. 2. PQ power capability curve for PV-DERs.

using the statistical methods adapted from a previous study [38]. The purpose was to measure the performance effectiveness of each proposed control strategy as shown in the following subsections:

- Active and reactive power output of inverter

The relationship between active and reactive power was determined based on PQ quadrant in Figure 2. The setting of SI based on unity PF allowed the active power dispatched in PV system to reach its maximum value according to the nominal VA rating of inverter. However, it was challenging to achieve the maximum active power dispatched due to meteorological factors and inverter efficiency. The PV inverter was also discovered to be in voltage regulation mode and the limits of maximum active and reactive power depended on its size.

- Inverter loading index (ILI)

ILI was defined as the ratio of the total active and reactive power to the nominal power rating of inverter. It was used to describe the nominal power rating available to accommodate the compensated active and reactive power.

- Transformer loading index (TLI)

TLI was defined as the ratio of the load on the transformer to the nominal power rating. It was used to describe the input power received by transformer from the output of inverter. Moreover, the output of transformer was the total power flow to the grid.

- Voltage profile on pv system

The voltage metric evaluated was the daily voltage profile at LV and MV busbars of PV system. It was used to explain the statistics of the voltage in PV system over a specific period.

- Voltage Deviation Index (VDI) on Distribution Network

VDI was applied to assess the percentage deviation of the grid voltage from the nominal voltage. It was used to describe the level at which the grid voltage deviated from the nominal voltage over time.

- Power Losses

An increase in the active power supply and reactive power compensation led to more need to investigate power losses and this metric was used to determine the overall efficiency of distribution network operations.

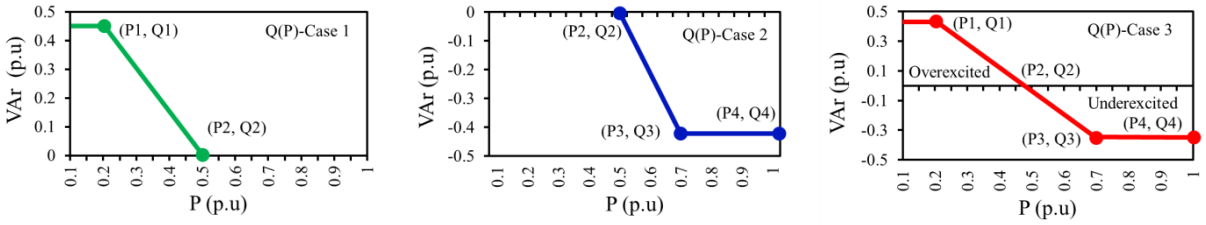

(a) (b) (c)

Fig. 3. Q(P) characteristic curve based on droop setting (a) case 1, (b) case 2, and (c) case 3.

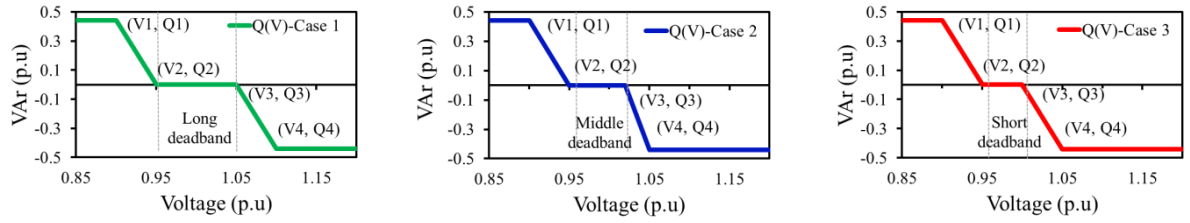

(a) (b) (c)

Fig. 4. Q(V) characteristic curve based on droop setting (a) case 1, (b) case 2, and (c) case 3.

2. Simulation Setup and Case Studies

2.1. Proposed Smart Inverter with Droop Setting

Inverter operating with a constant power factor (PF = 1) or PV without reactive power control was used as the base case. Therefore, the control strategies simulated are stated as follows:

- Q(P) characteristic
- Q(V) characteristic
- Combination of Q(V) and Q(P) characteristic

The characteristics of each control strategy depended on the setpoint of the active power or voltage with the minimum and maximum thresholds determined based on the droop setting scheme. Meanwhile, the minimum and maximum reactive power values were set based on the technical specifications of inverter provided by SI provider. It was observed that the minimum reactive power limit was set at 44% by the IEEE 1547 standard based on the categories of the DERs.

The characteristic curve for Q(P) control mode is presented in Figure 3 with a focus on three different setpoints. The Q(P) case-1 showed that the SI supplied both active and reactive power in Figure 3(a). The Q(P) case-2 indicated that the SI supplied active power and absorbed VAr in Figure 3(b) and Q(P) case-3 described the SI had the ability to supply both active and reactive power (injection/absorption) in Figure 3(c). A detailed description of Q(P) control setpoints is provided in Table 1. Meanwhile, the characteristic curve for Q(V) control mode is presented in Figure 4 and the Q(V) case-1 for long dead-band was identified in Figure 4 (a), Q(V) case-2 with middle dead-band in Figure 4(b), and Q(V) case-3 showing short dead-band in Figure 4(c). The comprehensive description of Q(V) control setpoints is also presented in Table 2.

A simple scheme of the proposed Q(V)-Q(P) combined control is presented in the following Figure 5 based on two stages. The first focused on inverter maintaining grid voltage limits by compensating for reactive power while the second showed that the control of reactive power compensation depended on the production of active power. The droop settings were applied based on the real-time voltage reference fed into inverter module while the effective reactive power was calculated according to voltage thresholds. This strategy was used to develop three different cases based on maximum active power limitations including Q(V)-Q(P) case-1 for SI without power limits, Q(V)-Q(P) case-2 for SI with 80% active power limit, and Q(V)-Q(P) case-3 for SI with 70% active power limit.

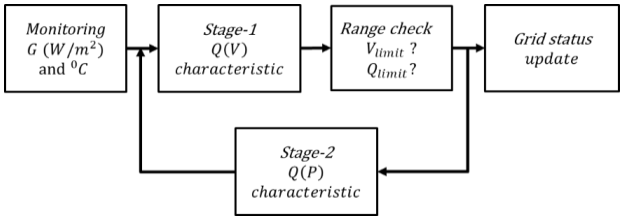

Fig. 5. Q(V)-Q(P) combined control scheme

Table 1. Details of the setting point for Q(P) control mode

Q(P)	(P_1, Q_1)	(P_2, Q_2)	(P_3, Q_3)	(P_4, Q_4)
Case-1	(0.2, 0.44)	(0.5, 0)	(0, 0)	(0, 0)
Case-2	(0, 0)	(0.5, 0)	(0.7, -0.44)	(1.0, -0.44)
Case-3	(0.2, 0.44)	(0.5, 0)	(0.7, -0.44)	(1.0, -0.44)

Table 2. Details of the setting point for Q(V) control mode

Q(V)	(V_1 , Q_1)	(V_2 , Q_2)	(V_3 , Q_3)	(V_4 , Q_4)
Case-1	(0.90, 0.44)	(0.95, 0)	(1.05, 0)	(1.1, -0.44)

Case-2	(0.90, 0.44)	(0.95, 0)	(1.02, 0)	(1.05, -0.44)

Case-3	(0.90, 0.44)	(0.95, 0)	(1, 0)	(1.05, -0.44)

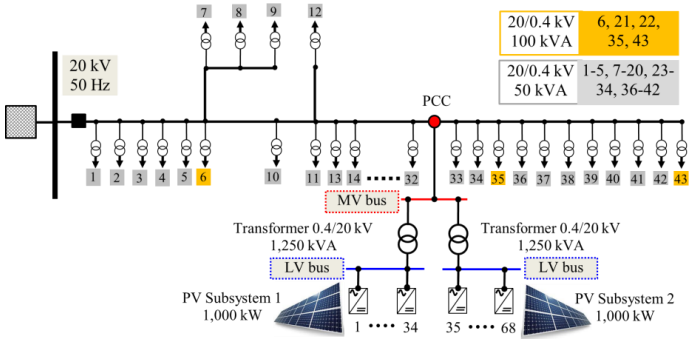

Fig. 6. Single line diagram of the radial distribution network with solar PV multi-smart inverter.

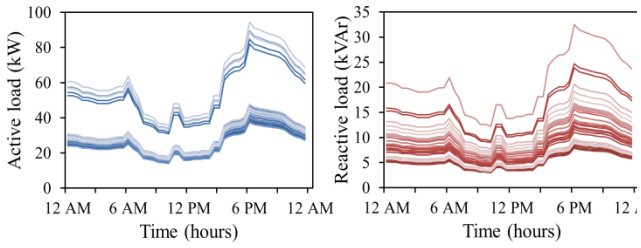

(a) (b)

Fig. 7. Load profile on 43 bus distribution network at (a) active load and (b) reactive load.

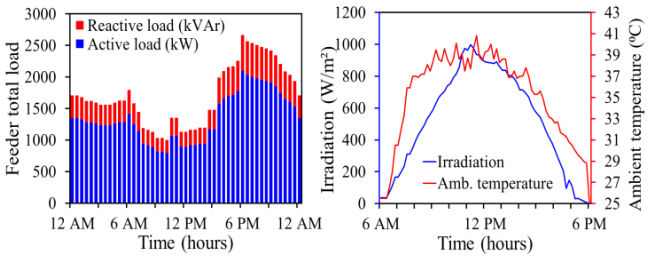

(a) (b)

Fig. 8. Daily profile of the (a) feeder total load and (b) solar irradiation and ambient temperature.

2.2. Distribution Network Test

The benefits of the proposed strategy were assessed through the simulations conducted on a real medium-voltage distribution network in Gorontalo, Indonesia. The simplified single-line diagram of the 43-bus system used for the test is presented in Figure 6 with a total of 2,000 kW PV plant connected to the MV grid between bus 32 and bus 33. Moreover, the feeder received its main power supply and voltage from the substation. The configuration of the multi-smart inverter PV plant system connected in parallel to distribution network is also indicated in Figure 6. It was discovered that PV plant had two subsystems and each had a capacity of 1,000 kW, 34 inverter units with a nominal rating of 33.12 kVA, and connected to a 1,250 kVA power transformer.

The feeder load fluctuated over a 24-hour period with heavy loads at night and light loads in the morning. The active load curve for the 43 buses is presented in Figure 7a

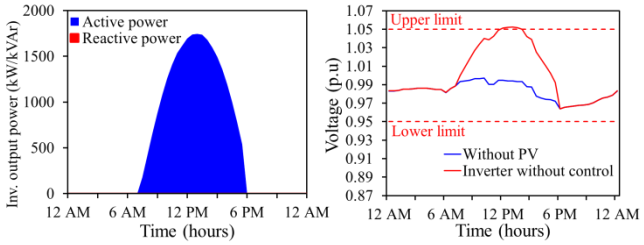

(a) (b)

Fig. 9. Daily profile for the (a) inverter output power and (b) voltage at PCC.

while the reactive load is in Figure 7b. Moreover, a bar chart was developed for the total feeder load over 24 hours with a 30-minute time interval in Figure 8a. The solar irradiations and ambient temperature data were recorded on May 3, 2023 and the resulting curves are shown in Fig. 8b.

3. Impact of Inverter PV Without Control

The power flow analysis was conducted with consideration for the real-time P-Q load profiles over 24 hours and inverter's output power for 12 hours. The daily profile of the total active power output from inverter without the reactive power is presented in Figure 9a. Based on meteorological data and 95% inverter power efficiency showed that the peak active power output of inverter was 1,744 kW. It was important to state that the PV plant did not operate at night due to the absence of a energy storage system. Moreover, the daily voltage profiles at PCC were compared before and after the integration of PV system without reactive power as shown in Figure 9b. The blue curve showed the maximum voltage was 0.997 p.u. at 10:00 am while the minimum was 0.963 p.u. at 6:00 pm. This was observed to be due to the existence of light loads in the morning and peak loads at night. Furthermore, the daily voltage profile at the PCC after the integration of PV system without reactive power control is presented in the red curve. It was discovered that PCC voltage experienced a significant increase (Vg ≥ 1.05 p.u.) from 12:00 pm to 1:30 pm and this peak PV power period led to voltage violations in distribution network. Daily voltage profiles were also compared for the 43 bus loads before and after PV introduction in Figures 10a and 10b and the voltages from bus 32 to bus 43 were observed to have exceeded 1.05 p.u.

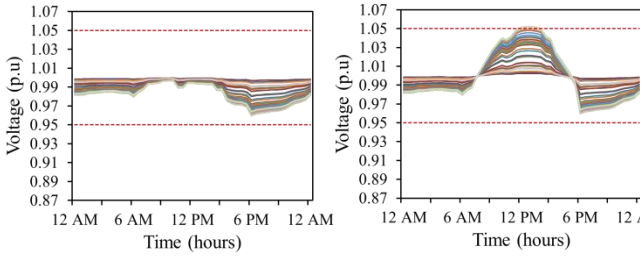

(a) (b)

Fig. 10. Voltage profile on 43-bus radial distribution network (a) without PV and (b) PV without control.

4. Simulation Results and Discussion

4.1. PV System Performance Metrics

The parallel inverters in subsystems 1 and 2 of PV produced all the total power from all inverter units. The simulation results for SI with Q(P) control mode are presented in Figure 11. It was discovered that Q(P) case-1 had a total peak reactive power injection of 937.6 kVAr during low radiation periods but did not inject or absorb any when the active power production increased beyond 1,000 kW, as shown in Figure 11a. The results also showed that the inverters in Q(P) case-2 only absorbed reactive power without injecting when the active power production exceeded 50% of nominal active power and the maximum total reactive power absorption was found to be -991 kVAr, as shown in Figure 11b. Meanwhile, Q(P) case-3 showed that inverter played dual roles by injecting active power and injecting or absorbing reactive power depending on the conditions, as presented in Figure 11c.

The performance of active and reactive power in Q(V) control mode is presented in Figure 12. It was observed that the differences in the voltage dead-band thresholds served as the requirements for the dynamic response of the reactive power supplied or absorbed by the SI for the three cases considered. Q(V) case-1 showed a long dead-band characteristic that led to a maximum total reactive power absorption of -321 kVAr in Fig. 12a. Q(V) case-2 indicated a middle dead-band characteristic with the ability to absorb a maximum of -775.6 kVAr in Fig. 12b. Meanwhile, Q(V) case-3 displayed a short dead-band characteristic capable of absorbing a maximum of -991 kVAr as presented in Fig. 12c. The results showed that the short dead band had a more significant sensitivity to absorbing reactive power compared to the long dead band. It was also discovered that reactive power was not supplied in all the cases of Q(V) control with the inverters observed to be producing only active power.

Figure 13 compares the total active and reactive power output by PV system to the grid using Q(V)-Q(P) combined control with a focus on the three distinct cases used to represent low-sensitivity, middle-sensitivity, and high-sensitivity responses from inverter. The results showed that the maximum reactive power output in case-1 during cloudy periods was 755 kVAr while a significant increase of -1146.8 kVAr was absorbed during clear periods as presented in Figure 13a. Meanwhile, case-2 showed a maximum active power output of 1621.6 kW and a maximum reactive power absorption of -1052.4 kVAr in Figure 13b. It was also discovered in Figure 13c that the maximum active power output in case-3 was 1420.4 kW and the maximum reactive power absorption was -870.2 kVAr. This was particularly evident during sunny periods when solar irradiance was at its peak and the active power limit was associated with the droop setting requirements. However, the metrics affecting the performance of active and reactive power in PV system are discussed in the following subsection.

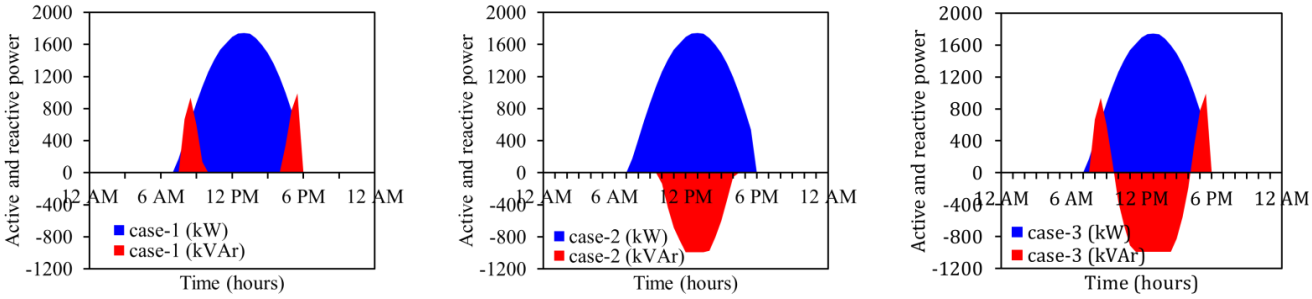

(a) (b) (c)

Fig. 11. Total active and reactive power output in PV inverter with Q(P) control mode (a) case-1, (b) case-2, and (c) case-3.

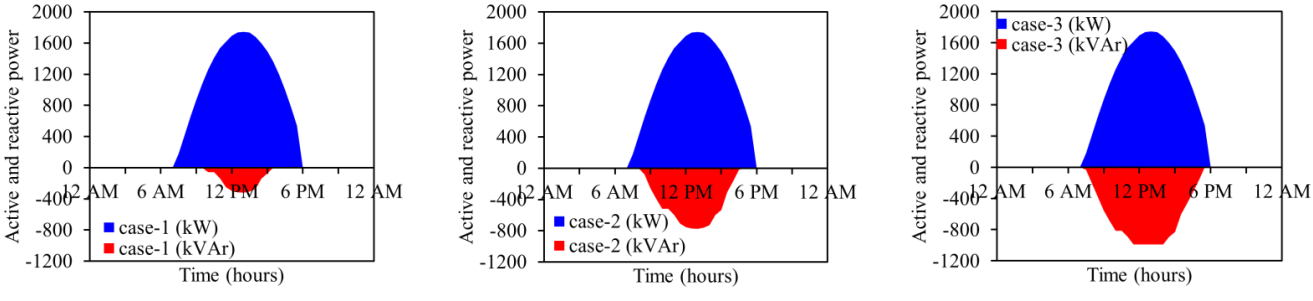

(a) (b) (c)

Fig. 12. Total active and reactive power output in PV inverter with Q(V) control mode (a) case-1, (b) case-2, and (c) case-3.

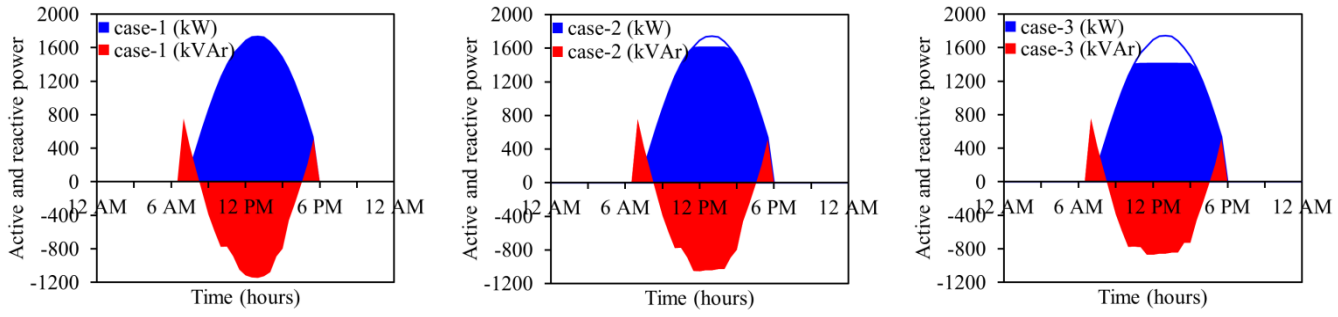

(a) (b) (c)

Fig. 13. Total active and reactive power output in PV inverter with Q(V)-Q(P) combined control (a) case-1, (b) case-2, and (d) case-3.

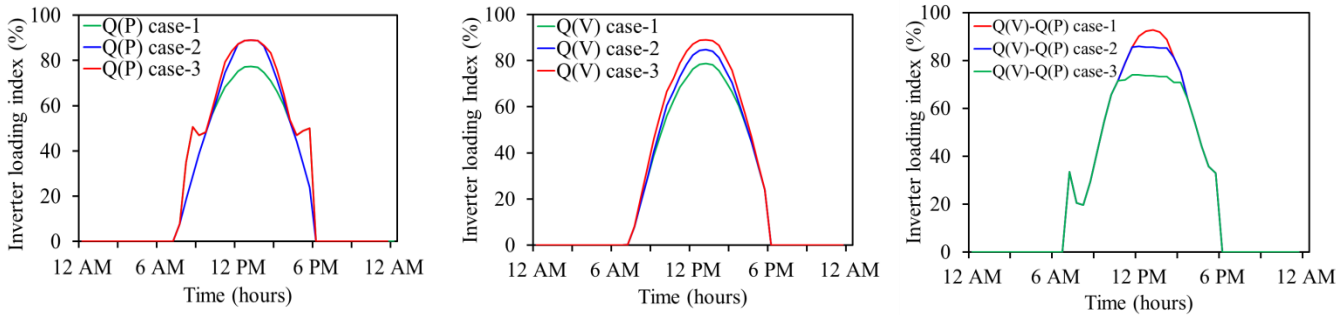

(a) (b) (c)

Fig. 14. Comparison of the inverter loading index for (a) Q(P); (b) Q(V); and (c) Q(V)-Q(P).

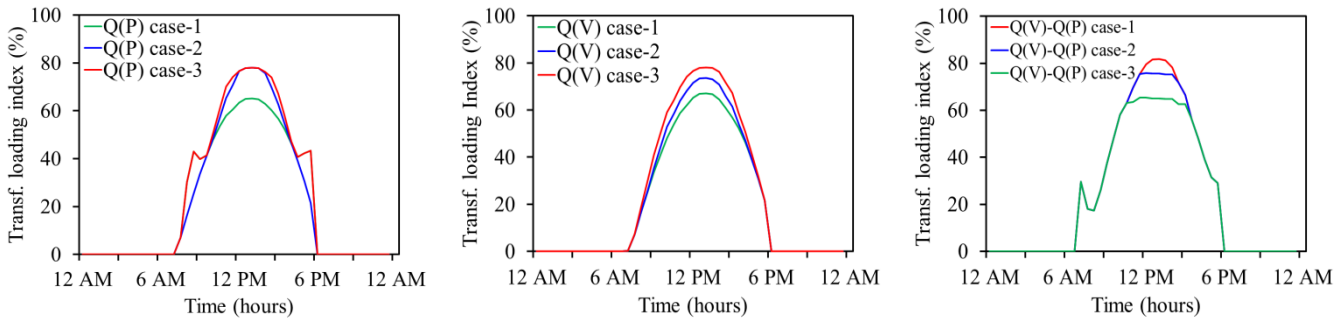

(a) (b) (c)

Fig. 15. Comparison of the transformer loading index for (a) Q(P); (b) Q(V); and (c) Q(V)-Q(P) combined controls.

4.2. Impact of Loading Index on PV System

This subsection was used to discuss the results for the loading indices in PV system with different modes of reactive power control. The percentage of inverter loading index (ILI) for the Q(P), Q(V), and Q(V)-Q(P) control modes is shown in Figure 14. The ILI in Q(P) mode with three different cases is compared in Figure 14a. The results showed that the highest ILI was recorded in case-2 and case-3 at 89.06% and the lowest was 77.43% in case-1. Increased inverter loading index due to high reactive power absorption. The ILI for Q(V) mode with three different cases is compared in Figure 14b. The results show that the highest ILI of 89.06% was recorded in case-3 followed by 84.74% in case-2, and the lowest was 78.33% in case-1. Furthermore, the ILI was in Q(V)-Q(P) with three different cases are compared in Figure 14c. It is known that the percentage of ILI increased significantly for case-1 is 92.67%, case-2 is 85.83%, and case-3 is 73.96%. This is due to limitations in the active power of the inverter. However, this condition shows that the inverter optimizes the rated capacity to absorb reactive power without overloading.

The percentage of transformer loading index (TLI) for Q(P), Q(V), and Q(V)-Q(P) control modes is shown in Figure 15. The TLI for Q(P) mode with three different cases is compared in Figure 15a. The results show that the characteristics of TLI are similar to ILI in Figure 14a with the highest value recorded in cases 2 and 3 to be 78.09% while in case-1 had 65.16%. The value in all the cases were below 80% and this showed transformer had sufficient capacity and was categorized as safe. The TLI percentage for Q(V) mode is shown in Figure 15b. The results show that the percentage of TLI in case-1, case-2, and case-3 was recorded at 67.09%, 73.60%, and 78.09%, respectively. Meanwhile, the percentage

of TLI in the combined control Q(V)-Q(P) with three different cases is compared in Figure 15c. The TLI for case-1 was found to be in a critical condition and required to be considered during the absorption of higher levels of reactive power. This could lead to an increase in thermal overloading of the cables and transformers, thereby showing the need for larger-sized cables and transformers to avoid the situation. The application of the maximum active power limit in case-2 and case-3 was observed to have led to a significant reduction in TLI percentages. The all results were considered important because the measurement of the loading indices could be used by PV operators to optimize the operations and keep transformer loading in safe limits.

4.3. Impact of the Voltage Metric on PV System

The results of the daily voltage profiles in PV system at different control modes are presented in this subsection with a focus on LV and MV buses. LV bus was used to represent the combined panel in PV system with multiple inverter connected to LV transformer. Meanwhile, MV bus was the switchgear on HV transformer connected to distribution network. The red curves in Figs.16a-b showed a significant increase in voltage for Q(P) case-1 and Q(V) case-1. This was found to be in line with the observation that there was a relationship between the amount of reactive power compensation and voltage fluctuations at LV and MV buses during the assessment of the PV performance metrics. Moreover, the application of Q(V)-Q(P) combined control in Fig.16c led to a stable voltage for the LV bus at 1.02 p.u. It was also discovered in Fig.17c that MV bus voltage was based on the loading characteristics of transformer. The results were considered important due to the influence of the droop setting sensitivity on the characteristics of the voltage in PV system. Therefore, daily voltage profiles were required to be applied to overvoltage trip (OVT) and undervoltage trip (UVT) devices on the main distribution panel by PV operators.

4.4. Impact of Voltage Metrics on Distribution Network

The Indonesian grid code requires that the connection of renewable energy generator should not cause more than a 5% VDI at PCC under normal conditions. Moreover, the power factor at PCC is required to be maintained in a range of 0.95 p.u for lagging or leading. The inability to fulfill these conditions indicates the need for PV system to operate with voltage regulation or reactive power control. The results of the power flow analysis for the three cases in Q(P) control mode are presented in Figure 18. It was discovered that VDI on distribution network significantly increased by 5% for case-1 in Fig.18a but stayed under 5% across all buses for case-2 and case-3 in Fig.18b and Fig.18c, respectively.

A similar observation was prepared with Q(V) control mode at different voltage dead-bands in Figure 19. Inverter with a long dead-band droop setting had high voltage sensitivity as presented in Fig.19a while the shortening of dead-band reduced VDI due to reactive power factors in Fig.19b and Fig.19c. Moreover, the impact of Q(V)-Q(P) combined control on VDI in the distribution network is shown in Figures 20(a-c) with the three cases tested used to represent low, middle, and high response, respectively. Case-1 showed lower VDI compared to single controls Q(V) and Q(P). It was also observed that the response of inverter in case-2 and case-3 suppressed deviations in distribution network due to the sensitivity of the voltage to changes in active and reactive power.

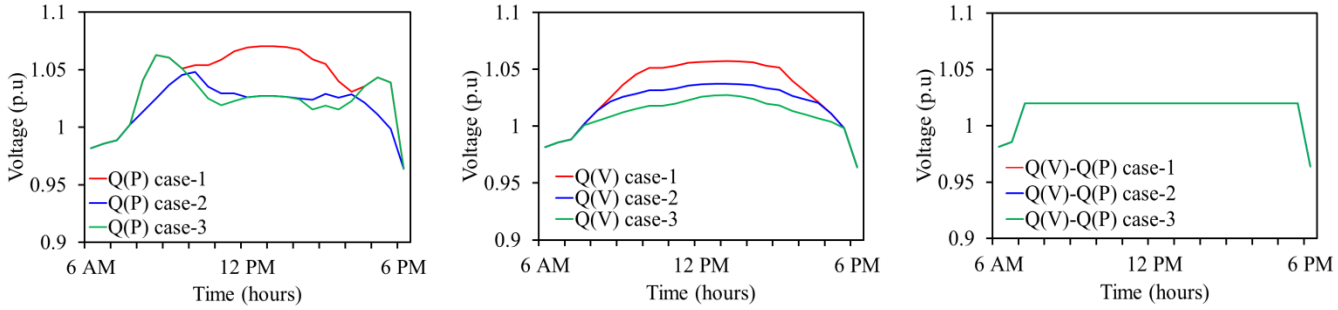

(a) (b) (c)

Fig. 16. Voltage profile on LV bus for (a) Q(P), (b) Q(V), and (c) Q(V)-Q(P) combined controls.

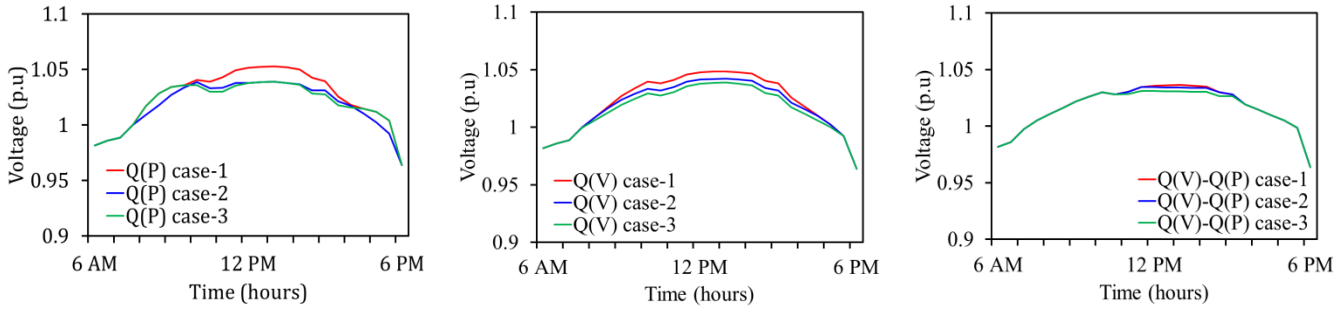

(a) (b) (c)

Fig. 17. Voltage profile on MV bus for (a) Q(P), (b) Q(V), and (c) Q(V)-Q(P) combined controls.

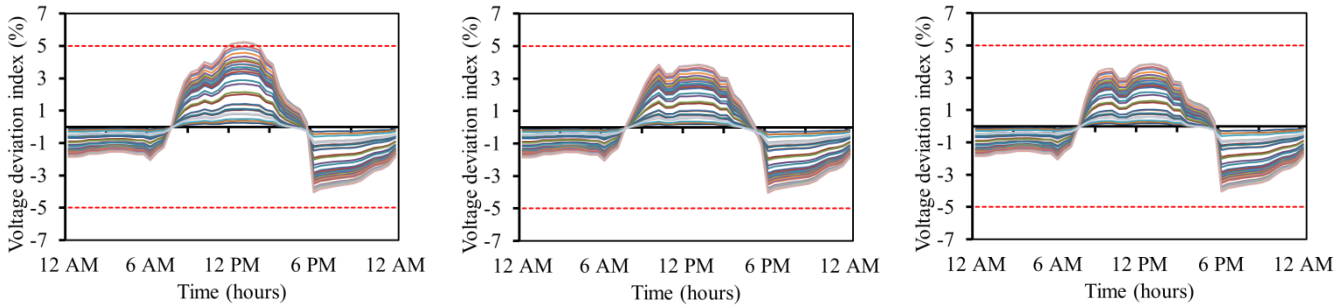

(a) (b) (c)

Fig. 18. Voltage deviation index on 43-bus radial distribution network with PV inverter using Q(P) control mode (a) case-1, (b) case-2, (c) case-3.

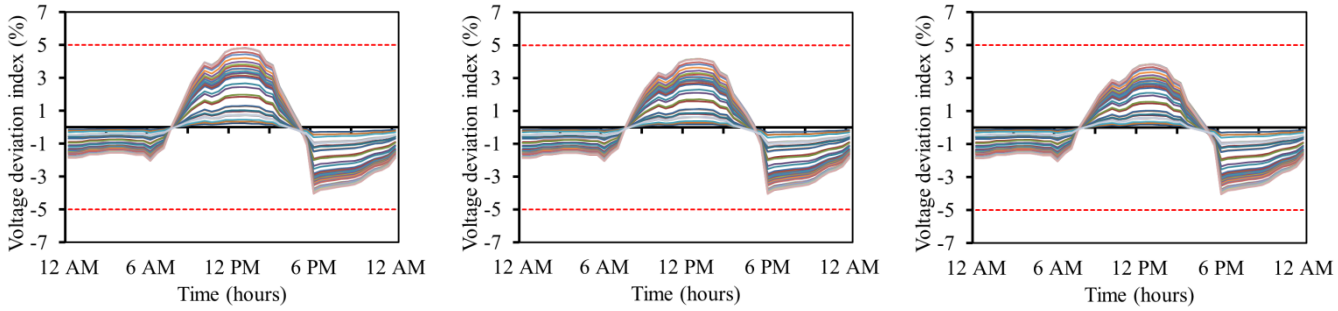

(a) (b) (c)

Fig. 19. Voltage deviation index on 43-bus radial distribution network with PV inverter using Q(V) control mode (a) case-1, (b) case-2, (c) case-3.

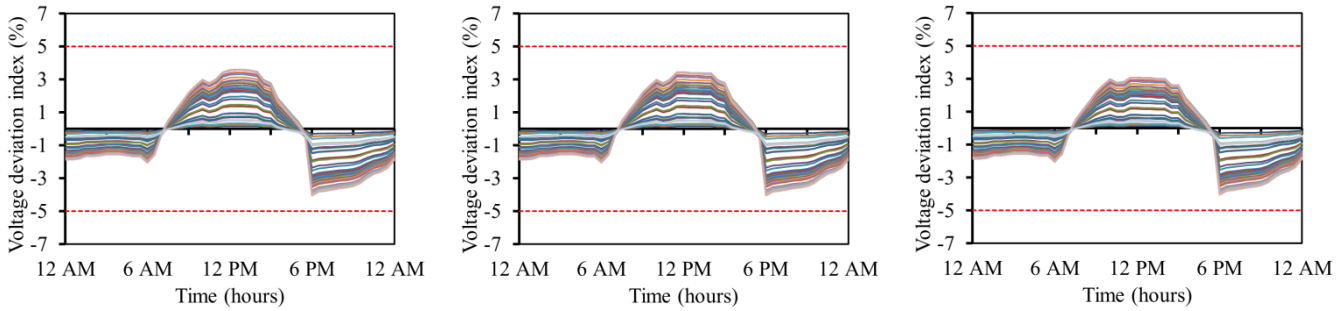

(a) (b) (c)

Fig. 20. Voltage deviation index on 43-bus radial distribution network with PV inverter using Q(V)-Q(P) combined control (a) case-1, (b) case-2, (c) case-3.

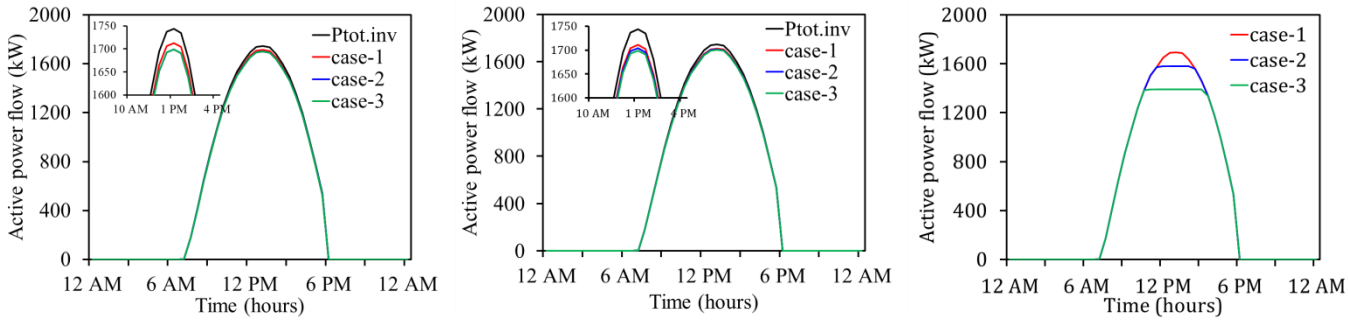

(a) (b) (c)

Fig. 21. Active power flow in PV system with (a) Q(P), (b) Q(V), and (c) Q(V)-Q(P) combined controls.

Table 3. Detailed comparison of percentage losses in PV systems

Time	Q(P)			Q(V)			Q(V)-Q(P)		
	Case-1	Case-2	Case-3	Case-1	Case-2	Case-3	Case-1	Case-2	Case-3
11:00 am	1.60	2.04	2.34	1.63	1.94	2.31	2.30	2.30	2.08
11:30 am	1.67	2.28	2.50	1.74	2.11	2.50	2.59	2.59	2.20
12:00 pm	1.74	2.53	2.53	1.84	2.21	2.53	2.74	2.60	2.20
12:30 pm	1.78	2.56	2.56	1.88	2.27	2.56	2.80	2.58	2.18
01:00 pm	1.79	2.57	2.57	1.90	2.28	2.57	2.82	2.58	2.18
13:30 pm	1.78	2.56	2.56	1.88	2.26	2.56	2.78	2.56	2.17
14:00 pm	1.73	2.50	2.53	1.81	2.18	2.53	2.67	2.56	2.17
14:30 pm	1.67	2.24	2.52	1.70	2.00	2.33	2.36	2.36	2.02
15:00 pm	1.57	1.92	2.20	1.59	1.85	2.21	2.17	2.17	2.02

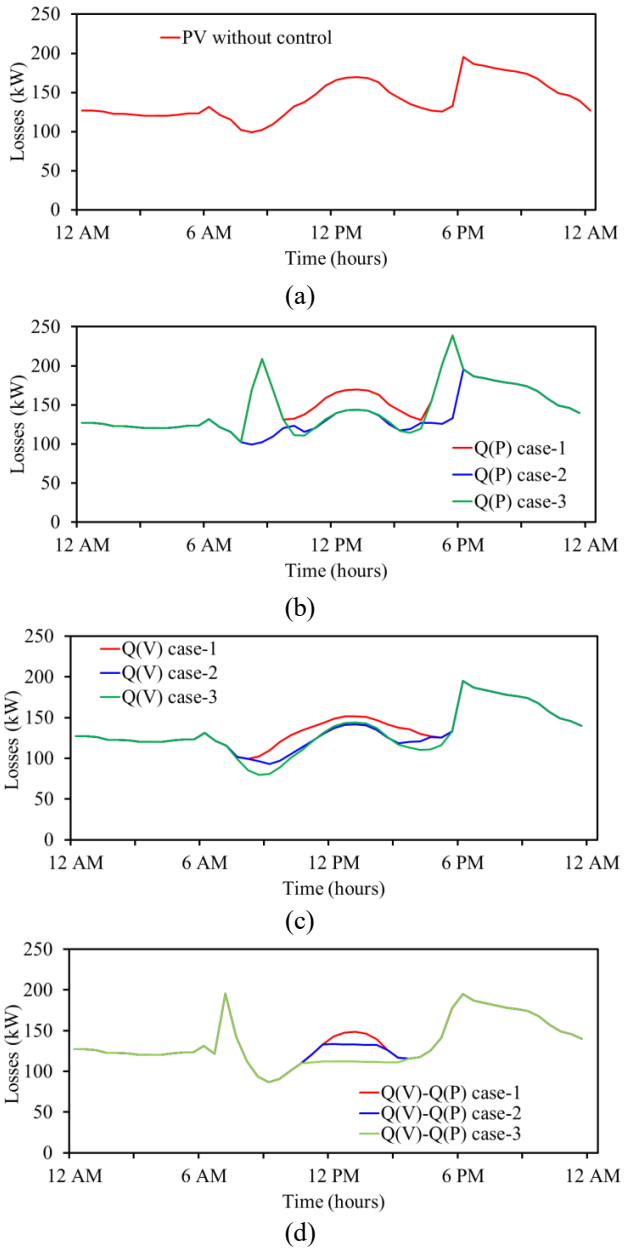

Fig. 22. Comparison of total power losses at (a) Constant PF = 1, (b) Q(P) control mode, (c) Q(V) control mode, and (d) Q(V)-Q(P) combined control.

4.5. Impact of Power Losses

Resistance and reactance factors in the PV system can result in power losses being exported to the grid. The total active power delivery has decreased due to these factors as shown in Figures 21(a-c), comparison of the power flow results for the three control modes. However, new facts were discovered that different control modes have resulted in different power losses. Details of the percentage of active power losses in the PV system are shown in Table 3. The percentage of losses is calculated based on the ratio of the total active power flow measured on the MV bus to the total active power output of the inverter measured on the LV bus. These results show a relationship between high reactive power absorption and increased power losses in the PV system.

A comparison of the daily total power losses for all control modes is shown in Figure 22 with different characteristics identified for each applied case. Figure 22a shows the active power losses profile for the base case inverter without reactive power control. Figures 22b, 22c, and 21d show a comparison of active power losses profiles for each Q(P), Q(V), and Q(V)-Q(P) combined control modes, respectively. The results show that characteristic losses are greater when the reactive power supply increases higher, especially when the PV module receives low solar radiation and inverter produces low active power. In addition, the combined control mode results in reduced power losses when the active power output of the inverter reaches the set point limit. However, it is important to consider that limiting active power can result in financial losses for PV owners.

5. Conclusion

Voltage violations due to the high penetration of PV power generator into distribution network made it impossible to comply with the grid code. This led to the introduction of active and reactive power control in smart inverter technology to manage voltage on distribution network. This study proposed a strategy to combine Volt-VAr and Watt-VAr control based on droop settings and compared its performance with single control strategies. The active power in PV system was evaluated based on solar irradiance and environmental temperature while the reactive power compensation was determined through the grid voltage. The quantity of the reactive power was influenced by the active power production and inverter size. The proposed control modes were based on

the droop settings in line with the characteristic curves of Q(P) and Q(V) commonly used. The results showed that the performance of the active and reactive power as well as the voltage in PV system changed according to the characteristics of each control strategy applied. This was because the increased reactive power supply or absorption led to a significant increase in inverter and transformer loading indices when the Volt-VAr and Watt-VAr controls were combined. However, these indices could be reduced by applying a maximum active power limit to SI. The maximum VDI in distribution network was significantly reduced to values under 5% and voltage violations can be anticipated. Power losses will increase when the inverter provides reactive power support. The higher active power limits can reduced the quantity of PV energy exports. It was recommended that future relevant studies on PV system with a combination of Volt-Watt-VAr control should consider the impact of this mode on reactive power compensation costs. Then propose solutions to reduce losses for distribution network operators and PV owners.

Acknowledgments

This work has been funded by the Indonesian Ministry of Education and Culture under the programme of Regular Fundamental Research Grants 2023. The authors are grateful to the Higher Education Service Institute (LLDIKTI XVI Gorontalo) and the UNISAN research institute for supporting to this research.

References

[1] IRENA (International Renewable and E. Agency), Renewable Energy Statistic 2023. 2023.

[2] IESR, “Indonesia Energy Transition Outlook 2023: Tracking Progress of Energy Transition in Indonesia: Pursuing Energy Security in the Time of Transition,” 2021.

[3] A. S. Akinyemi, K. Musasa, and I. E. Davidson, “Analysis of voltage rise phenomena in electrical power network with high concentration of renewable distributed generations,” Nature Scientific Reports, vol. 12, no. 1, pp. 1–22, 2022

[4] E. A. Hamza, B. E. Sedhom, and E. A. Badran, “Impact and assessment of the overvoltage mitigation methods in low-voltage distribution networks with excessive penetration of PV systems: A review,” International Transactions on Electrical Energy Systems, vol. 31, no. 12, pp. 1–31, 2021

[5] A. M. Colak and K. Kayisli, “Reducing voltage and frequency fluctuations in power systems using smart power electronics technologies: A review,” 9th International Conference on Smart Grid, icSmartGrid 2021, pp. 197–200, 2021

[6] A. Cabrera-Tobar, E. Bullich-Massagué, M. Aragüés-Peñalba, and O. Gomis-Bellmunt, “Active and reactive power control of a PV generator for grid code compliance,” Energies, vol. 12, no. 20, 2019

[7] P. A. V. Pato, F. C. L. Trindade, and X. Wang, “Hosting high PV penetration on distribution feeders with smart inverters providing local var compensation,” Electric Power Systems Research, vol. 217, no. January, p. 109168, 2023

[8] D. Iioka, T. Fujii, D. Orihara, T. Tanaka, T. Harimoto, A. Shimada, T. Goto, M. Kubuki, “Voltage reduction due to reverse power flow in distribution feeder with photovoltaic system,” International Journal of Electrical Power and Energy Systems, vol. 113, no. November 2018, pp. 411–418, 2019

[9] IEEE Std 1547, “IEEE Standard for Interconnection and Interoperability of Distributed Energy Resources with Associated Electric Power Systems Interfaces,” IEEE standards. pp. 1–138, 2018.

[10] Kementrian ESDM, “Aturan Jaringan Sistem Tenaga Listrik (Indonesian Grid-Code),” Menteri Energi dan Sumber Daya Mineral Republik Indonesia, no. 3. pp. 417–607, 2020.

[11] K. Rahimi, A. Tbaileh, R. Broadwater, J. Woyak, and M. Dilek, “Voltage regulation performance of smart inverters: power factor versus volt-var control,” in North American Power Symposium (NAPS), Morgantown, Sep. 2017, pp. 1–6.

[12] I. A. Ibrahim and M. J. Hossain, “A benchmark model for low voltage distribution networks with PV systems and smart inverter control techniques,” Renewable and Sustainable Energy Reviews, vol. 166, no. June, p. 112571, 2022.

[13] N. Ninad, E. Apablaza-Arancibia, M. Bui, J. Johnson, S, Gonzalez, R, Darbali-Zamora, “PV inverter grid support function assessment using open-source IEEE P1547.1 test package,” Conference Record of the IEEE Photovoltaic Specialists Conference, vol. 2020-June, no. August, pp. 1138–1144, 2020.

[14] K. Luo and W. Shi, “Comparison of voltage control by inverters for improving the PV penetration in low voltage networks,” IEEE Access, vol. 8, pp. 161488–161497, 2020.

[15] A. Inaolaji, A. Savasci, and S. Paudyal, “Distribution grid optimal power flow in unbalanced multiphase networks with volt-var and volt-watt droop settings of smart inverters,” IEEE Transactions on Industry Applications, vol. 58, no. 5, pp. 5832–5843, 2022.

[16] A. M. Howlader, S. Sadoyama, L. R. Roose, and Y. Chen, “Active power control to mitigate voltage and frequency deviations for the smart grid using smart PV inverters,” Applied Energy, vol. 258, no. October 2019, p. 114000, 2020.

[17] A. O. Muhammed and M. Rawa, “A systematic PVQV-curves approach for investigating the impact of solar photovoltaic-generator in power system using powerworld simulator,” Energies, vol. 13, no. 10, 2020.

[18] M. K. Singh, S. Taheri, V. Kekatos, K. P. Schneider, and C. C. Liu, “Joint grid topology reconfiguration and

design of Watt-VAR curves for DERs," IEEE Power and Energy Society General Meeting, vol. 2022-July, pp. 1–5, 2022.

[19] G. Chandra Mahato, S. Ranjan Biswal, T. Roy Choudhury, B. Nayak, and S. Bikash Santra, "Review of active power control techniques considering the impact of MPPT and FPPT during high PV penetration," Solar Energy, vol. 251, no. September 2022, pp. 404–419, 2023.

[20] A. Ali, K. Mahmoud, D. Raisz, and M. Lehtonen, "Probabilistic approach for hosting high PV penetration in distribution systems via optimal oversized inverter with Watt-Var functions," IEEE Systems Journal, vol. 15, no. 1, pp. 684–693, 2021.

[21] K. Gholami, M. R. Islam, M. M. Rahman, A. Azizivahed, and A. Fekih, "State-of-the-art technologies for volt-var control to support the penetration of renewable energy into the smart distribution grids," Energy Reports, vol. 8, pp. 8630–8651, 2022.

[22] I. Afandi, A. P. Agalgaonkar, and S. Perera, "Integrated Volt/Var control method for voltage regulation and voltage unbalance reduction in active distribution networks," Energies, vol. 15, no. 6, 2022.

[23] Q. Li, Y. Zhang, T. Ji, X. Lin, and Z. Cai, "Volt/Var control for power grids with connections of large-scale wind farms: A Review," IEEE Access, vol. 6, pp. 26675–26692, 2018.

[24] F. Aboshady, O. Ceylan, A. F. Zobaa, A. Ozdemir, G. Taylor, and I. Pisica, "Sequentially coordinated and cooperative Volt/Var control of PV inverters in distribution networks," Electronics, vol. 12, no. 8, p. 1765, Apr. 2023.

[25] T. S. Ustun, J. Hashimoto, and K. Otani, "Impact of smart inverters on feeder hosting capacity of distribution networks," IEEE Access, vol. 7, pp. 163526–163536, 2019.

[26] D. Almeida, J. Pasupuleti, and J. Ekanayake, "Comparison of reactive power control techniques for solar pv inverters to mitigate voltage rise in low-voltage grids," Electronics (Switzerland), vol. 10, no. 13, pp. 1–16, 2021.

[27] T. Gush, C. H. Kim, S. Admasie, J. S. Kim, and J. S. Song, "Optimal smart inverter control for PV and BESS to improve PV hosting capacity of distribution networks using slime mould algorithm," IEEE Access, vol. 9, pp. 52164–52176, 2021.

[28] V. Sharma, M. H. Haque, S. M. Aziz, and T. Kauschke, "Smart inverter and battery storage controls to reduce financial loss due to overvoltage-induced PV curtailment in distribution feeders," Sustainable Energy, Grids and Networks, vol. 34, p. 101030, 2023.

[29] W. Ely, H. Hamza, and S. P. Betoka, "Energy management of an autonomous hybrid wind-photovoltaic microgrid with battery storage," 2023 12th International Conference on Renewable Energy Research and Applications (ICRERA), pp. 492–498, 2023.

[30] U. Cetinkaya, R. Bayindir, and S. Ayik, "Ancillary services using battery energy systems and demand response," in 9th International Conference on Smart Grid, icSmartGrid 2021, 2021, pp. 212–215.

[31] K. Gholami, A. Azizivahed, A. Arefi, and L. Li, "Risk-averse Volt-VAr management scheme to coordinate distributed energy resources with demand response program," International Journal of Electrical Power and Energy Systems, vol. 146, no. October 2022, 2023.

[32] I. Táczi, B. Hartmann, and I. Vokony, "Impact study of smart grid technologies on low voltage networks with high penetration of renewable generation," International Journal of Renewable Energy Research, vol. 10, no. 2, pp. 519–528, 2020.

[33] M. V. Kumar, R. S. S. Nuvvula, P. P. Kumar, N. H. Haroon, I. W. Suryasa, and U. Priya, "A Review on demand side management system and its computer control methods," in 2023 12th International Conference on Renewable Energy Research and Applications (ICRERA), 2023.

[34] S. Hashemi and J. Østergaard, "Methods and strategies for overvoltage prevention in low voltage distribution systems with PV," IET Renewable Power Generation, vol. 11, no. 2, pp. 205–214, 2017.

[35] C. Li, V. R. Disfani, H. V. Haghi, and J. Kleissl, "Coordination of OLTC and smart inverters for optimal voltage regulation of unbalanced distribution networks," Electric Power Systems Research, vol. 187, no. November 2019, p. 106498, 2020.

[36] H. A. Khan, M. Zuhaib, and M. Rihan, "Voltage fluctuation mitigation with coordinated OLTC and energy storage control in high PV penetrating distribution network," Electric Power Systems Research, vol. 208, no. March, p. 107924, 2022.

[37] L. Pizzimbone, "Impact of on-load tap changers and smart controllers on the distributed renewable energy hosting capacity," International Journal of Smart grid (ijSmartGrid), vol. 6, no. 4, pp. 132–135, 2023.

[38] P. P. Vergara, M. Salazar, T. T. Mai, P. H. Nguyen, and H. Slootweg, "A comprehensive assessment of PV inverters operating with droop control for overvoltage mitigation in LV distribution networks," Renewable Energy, vol. 159, pp. 172–183, 2020.

[39] S. Tuo, D. Jiandong, and X. Ma, "Active and reactive power coordination control strategy of overvoltage for distributed PV integrated grid," The Journal of Engineering, vol. 2019, no. 16, pp. 2960–2964, 2019.

[40] S. Yoshizawa et al., "Voltage-sensitivity-based Volt-VAR-Watt settings of smart inverters for mitigating voltage rise in distribution systems," IEEE Open Access Journal of Power and Energy, vol. 8, no. November, pp. 584–595, 2021.

[41] H. Karbouj, Z. H. Rather, and B. C. Pal, "Adaptive voltage control for large scale solar PV power plant considering real life factors," IEEE Transactions on Sustainable Energy, vol. 12, no. 2, pp. 990–998, 2021.
[42] M. Ivas, A. Marušić, J. G. Havelka, and I. Kuzle, "P-Q capability chart analysis of multi-inverter photovoltaic power plant connected to medium voltage grid," International Journal of Electrical Power and Energy Systems, vol. 116, no. May 2019, pp. 1–7, 2020.
[43] T. S. Ustun and Y. Aoto, "Analysis of smart inverter's impact on the distribution network operation," IEEE Access, vol. 7, pp. 9790–9804, 2019.